ACS APPLIED MATERIALS & INTERFACES

Letter

www.acsami.org

Shape Control of Ag Nanostructures for Practical SERS Substrates

Tae Yoon Jeon,[†] Sung-Gyu Park,*[,‡] Su Yeon Lee,[†] Hwan Chul Jeon,[†] and Seung-Man Yang*[,†]

[†]National Creative Research Initiative Center for Integrated Optofluidic Systems; Department of Chemical and Biomolecular Engineering, Korea Advanced Institute of Science and Technology, 335 Gwahangno, Yuseong-gu, Daejeon, 305-701, Korea

[‡]Advanced Functional Thin Films Department, Korea Institute of Materials Science (KIMS), Changwon, Gyeongnam 641-831, Korea

Supporting Information

ABSTRACT: Large-area, highly ordered, Ag-nanostructured arrays with various geometrical features were prepared for use as surface-enhanced Raman scattering (SERS)-active substrates by the self-assembly of inorganic particles on an SU-8 surface, followed by particle embedding and Ag vapor deposition. By adjusting the embedding time of the inorganic particles, the size of the Ag nanogap between the geometrically separated hole arrays and bowl-shaped arrays could be controlled in the range of 60 nm to 190 nm. More importantly, the SU-8 surface was covered with hexagonally ordered nanopillars, which were formed as a result of isotropic dry etching of the interstices, leading to triangular-shaped Ag plates on nanopillar arrays after Ag vapor deposition. The size and sharpness of the triangular Ag nanoplates and nanoscale roughness of the bottom surface were adjusted by controlling the etching time. The potential of the various Ag nanostructures for use as practical SERS substrates was verified by the detection of a low concentration of benzenethiol. Finite-difference time-domain (FDTD) methodology was used to demonstrate the SERS-activities of these highly controllable substrates by calculating the electric field intensity distribution on the metallic nanostructures. These substrates, with high sensitivity and simple shape-controllability, provide a practical SERS-based sensing platform.

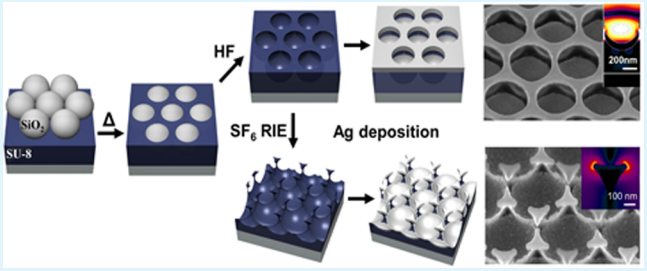

KEYWORDS: *surface-enhanced Raman scattering, nanowell array, nanopillar array, finite-difference time-domain, colloidal lithography*

INTRODUCTION

Surface-enhanced Raman scattering (SERS) spectroscopy, which uses random aggregates of metal nanoparticles or nanowires, has shown promise in the highly sensitive detection of various chemical and biological analytes.[1−10] However, the nonuniform distribution of "hot spots" and the randomly roughened metal surfaces that result in inhomogeneous distribution of target molecules provide challenges in regard to obtaining precisely controllable and reproducible SERS performance. To produce SERS-based chemical or biomolecular sensors for practical applications, researchers have developed periodic metal nanostructures using various lithographic techniques, including e-beam lithography,[11−13] and soft lithography.[14−16] However, a simple and reproducible method for the fabrication of metal nanostructures over a large area with high uniformity still remains a major issue. In this regard, nanosphere lithography and colloidal lithography, which use hexagonally ordered colloidal nanoparticles, are strong candidates for generating nanoscopic metal nanostructures with low fabrication costs and simple methodology.[17−20]

Nanogap sizes, sharpness, and the roughness of metal nanostructures are important geometrical factors that affect the Raman signal because of the highly enhanced electromagnetic (EM) fields that occur near small metal nanogaps and the lightning rod effect at sharp edges.[21−26] A method was previously reported that involved the generation of individual discs on pillar structures by using e-beam lithography and a reactive ion etching (RIE) process to tune metal nanogap size and resulting SERS enhancements.[27] In addition, a facile fabrication method for generating Ag spike arrays with sharp edges was suggested, where a self-organization process based on the condensation of water droplets and a vapor deposition procedure were used.[28]

In this article, we report a facile and versatile method for fabricating geometry-controllable SERS substrates, including Ag nanowell arrays and triangular shaped plates with sharp edges on the top of nanopillars. The procedure involved the trapping of the monolayer SiO_2 particles at an SU-8 resin/air interface (TIPSAI) via capillary wetting, followed by SF_6 RIE and Ag vapor deposition. Recently, we have demonstrated capillary wetting of multilayered colloidal crystals on the SU-8 resin for the fabrication of photonic microparticles.[29] However, in this report, we utilized the embedding of colloidal monolayer, RIE process, and a vapor deposition to produce various shapes of metal nanostructures. By controlling the embedding time of the SiO_2 particles and the RIE parameters for etching the SU-8

Received: November 27, 2012
Accepted: January 2, 2013
Published: January 2, 2013

Scheme 1. Schematic Diagram of the Generation of Hexagonally Ordered Ag Nanostructure Arrays with Various Shapes. (a) Formation of a Monolayer of SiO_2 Particles on the SU-8 Photoresist by Spin-Coating. (b) Embedding and Trapping of the SiO_2 Particles into the SU-8 Photoresist above the T_g of SU-8 Because of Capillary Wetting. (c) Formation of a Hexagonally Ordered SU-8 Well Array after Removing the SiO_2 Particles by HF Wet Etching. (d) Generation of Ag Nanowell Array by 100 nm Ag Vapor Deposition. (e) Generation of SU-8 Nanopillar Array by SF_6 RIE. (f) Formation of Ag Nanopillar Array by 100 nm Ag Vapor Deposition

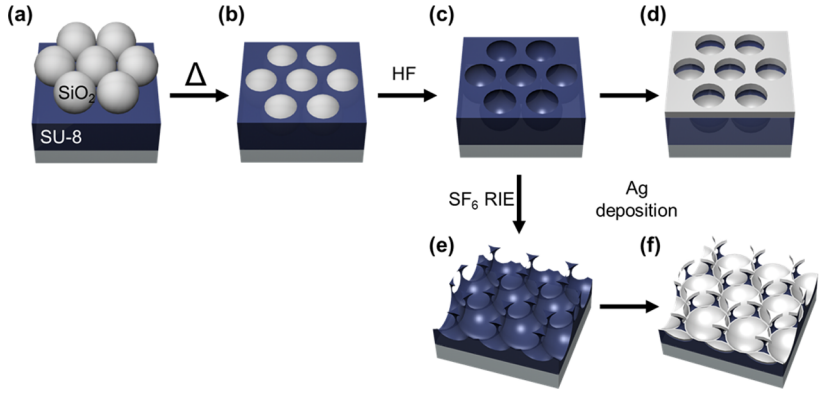

polymer, we were able to elucidate the effects of the various geometrical features, including nanogap size, sharpness, and roughness, on SERS performance. The Ag nanogap size was adjusted by simply varying the embedding time of the SiO_2 particles, and the sharpness and roughness of the Ag nanostructures could be altered by controlling the RIE parameters. The resulting Ag nanogap sizes and sharpened and roughened metallic edges provided highly enhanced EM fields due to localized surface plasmon resonance (LSPR).[22,23] The enhanced magnitude of the EM fields resulted in highly intensified Raman signals. The various Ag nanostructure arrays exhibited tunable SERS activities with Raman enhancement factors (EFs) on the order of 1×10^5, depending on the geometrical shape. Furthermore, such colloidal lithography-based Ag nanostructures could be fabricated over a large area with large-scale structural homogeneity and high density.

EXPERIMENTAL SECTION

Preparation of Hexagonally Ordered Nanowell Arrays. A 1.5-μm-thick layer of SU-8 photoresist was spin-cast onto an O_2 plasma-treated Si wafer (Scheme 1). Next, SiO_2 particles of 540 nm or 1 μm in diameter were synthesized using an oil and water interface to allow slow diffusion of precursors for generating highly monodisperse particles.[30] After ultrasonication for 12 h to remove particle aggregates, a 10 wt % colloidal suspension in ethanol was spin-coated onto the O_2 plasma treated SU-8 surface to form a hexagonally ordered colloidal monolayer over a large area. For obtaining the highly ordered colloidal array, adequate control of the spin speed (ranging from 3000 rpm to 5000 rpm) was required. The resulting samples were heated on a hot plate at 95 °C, which is above the glass transition temperature (T_g) of the SU-8, in order to embed the SiO_2 particles within the surface of the polymeric film by capillary wetting. After cooling to room temperature, wet etching with 5 wt % HF for 2 min was used to remove the particles leaving a nanowell array. The samples were washed thoroughly with water several times and kept in a fume hood to allow total evaporation of the solvent.

Fabrication of Ag Nanowell Arrays. A 100 nm thick Ag film was deposited on the top of the SU-8 nanowell arrays using an e-beam evaporator (Scheme 1d). To enhance adhesion between SU-8 substrate and Ag film, a thin layer of Cr (3 nm) was first deposited as an adhesion layer.

Fabrication of Ag Nanopillar Arrays. RIE using SF_6 (Vacuum Science VSRIE-400A) of the SU-8 nanowell array led to the creation of a hexagonal array of triangular shaped nanopillars (Scheme 1e). SF_6 gas was introduced into the chamber at a flow rate of 100 sccm, and the base pressure was maintained at 0.28 Torr with a RF power of 100 W. After the RIE process, a 100 nm thick Ag film was deposited for the fabrication of metallic triangular shaped nanoplates on the nanopillar array (Scheme 1f).

Treatment with Benzenethiol (BT). The various resulting metallic nanostructures were immersed into a 2 mM solution of BT in ethanol for 12 h. They were then washed with ethanol several times and dried under nitrogen gas.

Measurements and Characterization. The morphologies of the surfaces and cross sections of the resulting Ag nanostructures were investigated using field emission-scanning electron microscopy (FE-SEM, Hitachi S-4800). The Raman spectra of BT-adsorbed nanowell arrays were measured using a high-resolution dispersive Raman microscope (Horiba Jobin Yvon, LabRAM HR UV/Vis/NIR), in which a 633 nm laser with a power of 75 mW was focused on the sample surface, covering an area 1 μm in diameter. In the case of Ag nanopillar arrays, Raman spectra were collected over 0.1 s using a compact portable Raman system (Ocean Optics Inc., QE65000-RAMAN-KIT). A near infra-red (NIR) laser operated at 785 nm with a power of 350 mW was used to illuminate a sample area 1 mm in diameter.

RESULTS AND DISCUSSION

We previously reported a method to fabricate a perfectly hydrophobic surface using TIPSAI.[31] Here, we combined TIPSAI, SF_6 RIE, and Ag vapor deposition to fabricate SERS-active substrates with various geometrical shapes such as nanowell structures and triangular nanoplates with sharp edges on the pillars, as shown in Scheme 1. From the different shapes of the Ag nanostructures, we could elucidate the geometrical effects of metallic nanostructures on SERS intensity, including the size of the nanogap between the separated hole and bowl-shaped arrays, and the sharpness and roughness of the triangular shaped Ag pillar arrays. Colloidal particles are widely used to generate regular nanoscopic structures over large areas.[32−35] In this work, colloidal SiO_2 particles were embedded in the surface layer of a polymer film to serve as a template for the formation of a patterned array. After etching of SiO_2 particles and deposition of a 100 nm Ag film on the nanowell array using e-beam evaporation, Ag nanowell arrays were produced, as shown in Figure 1. Interestingly, the Ag bowl-shaped structures, which were deposited into the voids in the SU-8 film, were not connected to the Ag hole array at the top

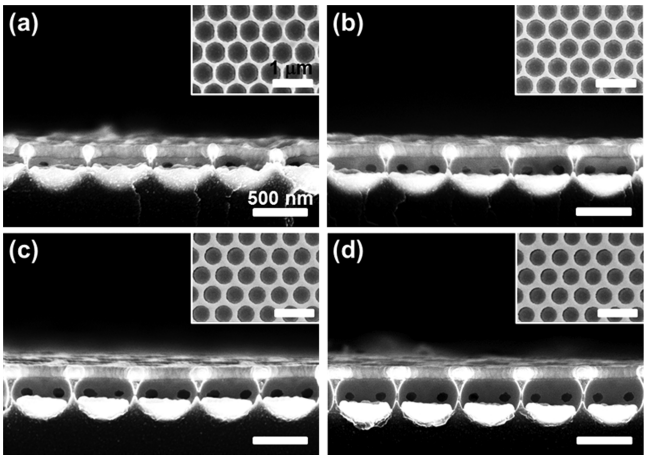

Figure 1. SEM images of resulting nanowell structures with various embedding times of SiO_2 particles within the surface of the polymeric film at 95 °C. (a) 5 s (d/a = 1.30), (b) 10 s (d/a = 1.42), (c) 20 s (d/a = 1.48), (d) 1 min (d/a = 1.54). Insets of a–d show top view of hexagonally ordered Ag nanowell array.

of the polymeric film; hence, these two separate layers of Ag provided a specific nanoscale gap. These results arose from the unidirectional deposition properties of the e-beam evaporation process.[18] Figure 1 shows cross-sectional SEM images of the resulting Ag nanowell arrays prepared with different SiO_2 embedding times of 5 s, 10 s, 20 s, and 1 min. The embedding depth (d) was increased from 350 nm to 415 nm as the embedding time was increased up to 1 min. However, d reached a maximum after 1 min embedding time (see the Supporting Information, Figure S1).[32] The size of the Ag nanogap between the top Ag nanohole array and the isolated Ag nanobowls increased from 60 nm up to 130, 160, and 190 nm with increasing embedding time. The precise size of the nanogaps could therefore be easily controlled by adjusting the heating time and temperature of the embedding process. Also, because SU-8 photoresist was used as the substrate material, colloidal lithography can be combined with photolithography to fabricate hierarchical structures (see the Supporting Information, Figure S2).

To verify the feasibility of using these fabricated samples as practical SERS substrates, we immersed the Ag nanostructured films with different sized nanogaps in an ethanolic solution of 2 mM BT for 12 h. Raman spectra of the surfaces were subsequently collected using a 633 nm HeNe laser source with 1 μm diameter, 75 mW power, and 10 s accumulation time. Figure 2 shows a comparison of the Raman intensity distribution obtained from the different Ag nanowell arrays. The spectra display peaks at 994, 1017, 1071, and 1571 cm^{-1}, which are the characteristic peak positions of BT.[8] Significantly higher Raman peak intensities can be clearly observed for the shorter embedding times. This phenomenon can be quantified by calculating the Raman EFs using the following equation

$$EF = (I_{SERS}/I_{Ref})(N_{Ref}/N_{SERS})$$

where I_{SERS} and I_{Ref} are the Raman intensities at a certain peak position (1071 cm^{-1} in this experiment) obtained from the fabricated metallic nanostructures with 99% bulk BT solution as a reference, and N_{Ref} and N_{SERS} are the number of BT molecules for the reference sample and SERS substrates. N_{Ref} was measured using a value of 1.073 g/cm^3 as the density of BT, and N_{SERS} was calculated from the ratio of the surface area

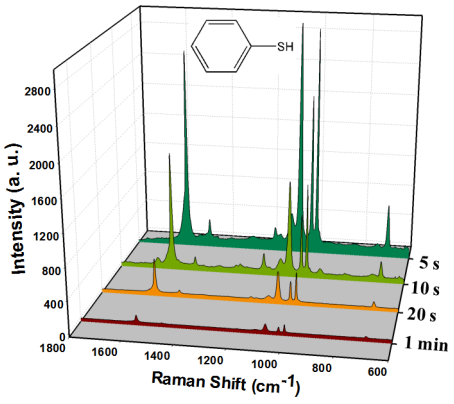

Figure 2. Raman scattering spectra of samples with different shapes of Ag nanowell arrays after immersion in 2 mM BT.

of Ag nanostructures to incident beam size (1 μm) using 6.86 × 10^{14} molecules/cm^2 as the value of the packing density of BT on the Ag surface.[36,37] The Raman EFs were calculated to be 2.64 × 10^5, 1.05 × 10^5, 3.33 × 10^4, and 8.24 × 10^3 at 5, 10, and 20 s and 1 min embedding time, respectively.

The electric field enhancement on the metallic nanostructures could be calculated using the finite-difference time-domain (FDTD) method. Figure 3 shows the electric field

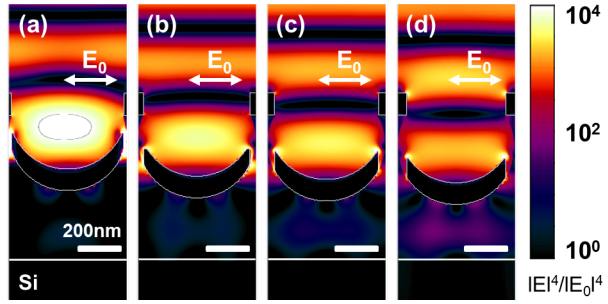

Figure 3. (a–d) Calculated electric field intensity distributions excited by an incident light with linearly polarized plane wave (λ = 633 nm) with different embedding times of 5, 10, and 20 s and 1 min, respectively. Maximum $|E|^4/|E_0|^4$ values of the structures are 1.38 × 10^4, 1.99 × 10^3, 1.0 × 10^3, and 7.58 × 10^2, respectively, which are proportional to the Raman signal intensity.

intensity distributions on excitation with a 633 nm wavelength of incident light, which corresponds to the wavelength of the experimental SERS measurements. In this calculation, the thickness of Ag film was assumed to be 100 nm and the incident light was linearly polarized, as described in Figure 3. From the calculated results, the electric field enhancement was strongly intensified in the case of 5 s embedding time because of resonance coupling of the nanogaps between the top of the Ag hole arrays and the bottom Ag bowl-like structures (Figure 3a). For the 5 s embedding time condition, a highly enhanced electric field was localized at both the edges of nanobowls and the center of the nanowells, resulting in strong Raman signals. Figure 3b–d also present the Ag nanogap effects on the enhancement of the local electric field. As embedding time increased, the size of the gap between the top and bottom Ag nanostructures increased, causing relatively weak plasmonic resonance at the center of the nanowells, even though the edges of the Ag nanobowls were still acting as "hot-spots". On the basis of the computed electric field intensity distributions, the

dx.doi.org/10.1021/am302874d | ACS Appl. Mater. Interfaces 2013, 5, 243–248

maximum $|E|^4/|E_0|^4$ values were found to be 1.38×10^4, 1.99×10^3, 1.0×10^3, and 7.58×10^2 from conditions of 5, 10, and 20 s and 1 min embedding time, respectively. Because SERS enhancements are proportional to the fourth power of EM enhancements ($|E|/|E_0|$),[38] it was possible to verify the transition of the experimental Raman intensity from FDTD simulation data. The trend in the analytical $|E|^4/|E_0|^4$ values, which decreased from 1.38×10^4 to 7.58×10^2 as a function of the embedding time, correlated well with the experimental Raman spectra, as shown in Figure 2. Such results indicate that our nanowell system does not require high-end advanced lithography or dry etching steps, unlike other reported fabrication procedures. Hence, our method can lead to inexpensive and straightforward route to produce SERS-active substrates with large-scale sample homogeneity.

The sharpness and roughness of the metallic structures are also important geometrical factors that are known to affect SERS activities.[22−26] To investigate such geometrical feature effects on SERS performance, we performed SF_6 RIE on the SU-8 nanowell arrays in order to change the shape of the nanostructures (from nanowell to nanopillar, Scheme 1e,f). Here, larger SiO_2 particles of 1 μm in diameter were used to increase the size of the interstice regions between nanowells. First, nanowell arrays were prepared with d/a = 1.6 by fully embedding the SiO_2 particles in the SU-8 for 5 min, followed by 100 nm of Ag deposition. Figure 4a shows an SEM image of

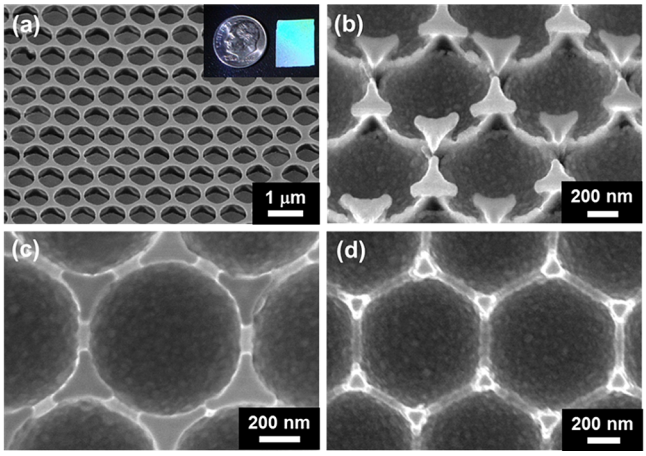

Figure 4. RIE effects on the surface geometry of the well array with d/a = 1.60. (a) Tilted (at 40°) SEM image shows hexagonally ordered Ag nanowell arrays after removal of the SiO_2 particles and subsequent deposition of 100 nm thick Ag. Inset of (a) shows 1 cm^2 area of Ag well array (US dime is shown for comparison). Uniform diffraction color is evidence of a large area of periodic pattern formation. (b) 40° tilted SEM image of a hexagonally ordered triangular plate on top of each of the nanopillars after 1 min of SF_6 RIE. Top views of the nanoplate array after (c) 1 min and (d) 2 min of SF_6 RIE.

the hexagonally ordered Ag nanowell array. This pattern also exhibited a uniform diffraction color over a large area on the centimeter scale, as shown in the inset of Figure 4a. After 1 min of SF_6 RIE, the surface was covered with hexagonally ordered triangular nanoplates on the top of the pillars, which were derived from the isotropic etching of the SU-8 interstices. After the subsequent deposition of 100 nm of Ag, triangular-shaped Ag nanoplates were obtained on the top of each of the nanopillars (Figure 4b−d). The nanostructures, with sides of 250 nm, were clearly disconnected from adjacent Ag nanotriangles (Figure 4b, c). By increasing the RIE time from 1 to 2 min, the size of the Ag triangular nanostructures decreased to 120 nm on each side, the vertices became sharper, and the three sides of each triangular nanostructure changed from curved to straight (Figure 4d). The RIE process also increased the surface roughness of the nanowell structures (see the Supporting Information, Figure S3). The density of the nanopillars was estimated to be $2.5 \times 10^8/cm^2$; however, it could be increased by simply using smaller SiO_2 particles as templates.

To investigate the effect of the RIE on the intensity of the Raman signal, we collected spectra using a compact portable Raman system. Although this particular instrument gave a relatively low spectral resolution, these spectrometers can be powerful analytical instruments when combined with nanostructured films that are able to significantly enhance the Raman scattering, making on-site, rapid, and accurate detection and identification of chemical and biological molecules possible. Figure 5 shows the RIE-dependent Raman spectra after

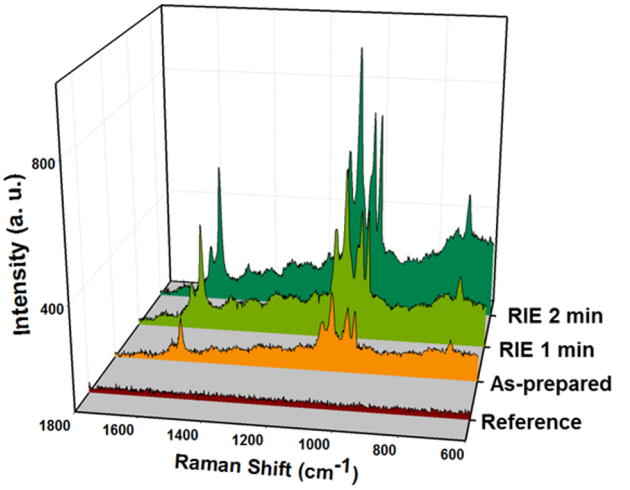

Figure 5. Raman scattering spectra of the different nanostructured surfaces after immersion in 2 mM BT.

immersion of the Ag nanostructured samples in 2 mM BT. Spectra were collected over 0.1 sec, using a NIR laser operated at 785 nm with a power of 350 mW. No characteristic peaks were detected on the smooth Ag film, which provided a reference surface for comparison. However, clear Raman scattering peaks were observed from the BT molecules in the presence of the Ag nanostructured film. Even though the size of each nanowell was large because of the 1-μm-diameter SiO_2 particles and the long embedding time, the Raman peaks were also detected from the Ag nanowell surface. The intensity of the Raman signals then increased with the RIE time.

After 1 min of RIE, the generation of triangular-shaped nanostructures with sharp edges contributed to a remarkable enhancement of the Raman signals compared with the Ag nanowell array. The edges of each nanoplate could function as 'hot-spots' to enhance the optical coupling effect of the EM field.[22,23] The nanoscale roughness on the bottom surface was seen to increase the Raman intensity further, which is in agreement with previous reports of nanoscale roughness producing beneficial effects on SERS enhancements.[24−26] After 2 min of SF_6 RIE, the intensity of the Raman signal was further increased. This phenomenon resulted from the more sharpened surfaces of three vertices, which is termed the lightning rod effect.[39,40] Such an effect on SERS enhancement

could also be described by using the FDTD method with proper approximations. Figure 6 shows the FDTD simulation

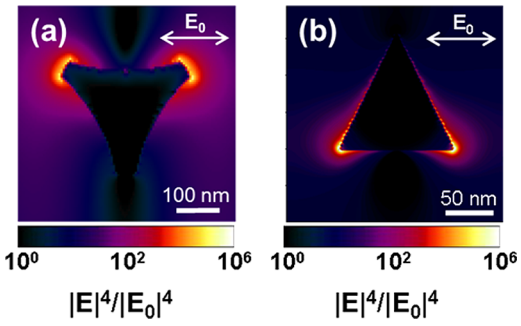

Figure 6. Calculated electric field intensity distributions with different shapes of Ag nanoplates of width (a) 250 nm and (b) 120 nm. Maximum $|E|^4/|E_0|^4$ values of the structures are 1.44×10^6 and 7.6×10^6, respectively, which are proportional to the Raman signal intensity. Arrows indicate the incident polarization direction.

results that demonstrate the electric field intensity distribution on the two types of triangular nanoplates excited by an incident light with linearly polarized planewave of 785 nm wavelength. Panels a and b in Figure 6 show the FDTD simulation results for the samples after 1 and 2 min RIE, respectively. From these simulation results, we observed that the local EM field was highly enhanced at the sharp edges of the Ag nanoplates and that the EM field confinement for the 2 min RIE sample was higher than that of the 1 min sample because of the sharper edges of the nanoplates. The calculated maximum $|E|^4/|E_0|^4$ values, which are proportional to SERS enhancement, increased from 1.44×10^6 to 7.6×10^6 with the increase in RIE time from 1 to 2 min. SERS performance could be also quantified by calculating the Raman EFs from the collected spectra. The estimated Raman EFs of the SU-8 nanobowl array, and the 1 and 2 min RIE samples, had values of 1.95×10^4, 7.04×10^4, and 1.36×10^5, respectively. The EF increase for the nanoplate array was attributed to both the generation of sharp features on the triangular pillars and the nanoscale roughness on the bottom surface.

CONCLUSIONS

In summary, various Ag nanostructures with controllable shapes were easily prepared by using a combination of self-assembly of inorganic particles on a polymeric surface, dry etching, and Ag vapor deposition processes. By controlling the embedding time of the SiO_2 particles and the RIE time for polymer etching, the effects of the nanogap size, sharpness, and roughness of Ag nanostructures on the enhancement of Raman signals were investigated. Furthermore, the effects of these geometrical features were clearly verified by FDTD simulation results. Because SU-8 photoresist was used as the substrate material, it is expected that the Ag nanostructures could be easily integrated into microfluidic chips by combining the procedure described here with conventional photolithography techniques.[41,42] This would provide a route to practical SERS-based optofluidic sensing devices.[43,44]

ASSOCIATED CONTENT

Supporting Information

Embedding depth of silica particles as a function of embedding time, fabrication of hierarchical structures by combining colloidal lithography and photolithography and roughness change of polymer surfaces with RIE time. This material is available free of charge via the Internet at http://pubs.acs.org

AUTHOR INFORMATION

Corresponding Author

*Phone: +82-55-280-3632 (S.-G.P.); +82-42-350-3962 (S.-M.Y.). Fax: +82-55-280-3570 (S.-G.P.); +82-42-350-5962 (S.-M.Y.). E-mail: sgpark@kims.re.kr (S.-G.P.); smyang@kaist.ac.kr (S.-M.Y.).

Notes

The authors declare no competing financial interest.

ACKNOWLEDGMENTS

This work was supported a grant from the Creative Research Initiative Program of the Ministry of Science and Technology for "Complementary Hybridization of Optical and Fluidic Devices for Integrated Optofluidic Systems". The authors also appreciated partial support from the Brain Korea 21 Program.

REFERENCES

(1) Nie, S. M.; Emery, S. R. *Science* **1997**, *275*, 1102−1106.
(2) Tao, A.; Kim, F.; Hess, C.; Goldberger, J.; He, R. R.; Sun, Y. G.; Xia, Y. N.; Yang, P. D. *Nano Lett.* **2003**, *3*, 1229−1233.
(3) Aroca, R. F.; Goulet, P. J. G.; Dos Santos, D. S.; Alvarez-Puebla, R. A.; Oliveira, O. N. *Anal. Chem.* **2005**, *77*, 378−382.
(4) Jackson, J. B.; Halas, N. J. *Proc. Natl. Acad. Sci. U.S.A.* **2004**, *101*, 17930−17935.
(5) Ko, H.; Tsukruk, V. V. *Small* **2008**, *4*, 1980−1984.
(6) Kneipp, K.; Haka, A. S.; Kneipp, H.; Badizadegan, K.; Yoshizawa, N.; Boone, C.; Shafer-Peltier, K. E.; Motz, J. T.; Dasari, R. R.; Feld, M. S. *Appl. Spectrosc.* **2002**, *56*, 150−154.
(7) Jang, S. G.; Choi, D. G.; Heo, C. J.; Lee, S. Y.; Yang, S. M. *Adv. Mater.* **2008**, *20*, 4862−4867.
(8) Hwang, H.; Kim, S. H.; Yang, S. M. *Lab Chip* **2011**, *11*, 87−92.
(9) Sun, Y. H.; Liu, K.; Miao, J.; Wang, Z. Y.; Tian, B. Z.; Zhang, L. N.; Li, Q. Q.; Fan, S. S.; Jiang, K. L. *Nano Lett.* **2010**, *10*, 1747−1753.
(10) Feng, H. J.; Yang, Y. M.; You, Y. M.; Li, G. P.; Guo, J.; Yu, T.; Shen, Z. X.; Wu, T.; Xing, B. G. *Chem. Commun.* **2009**, *15*, 1984−1986.
(11) Schuck, P. J.; Fromm, D. P.; Sundaramurthy, A.; Kino, G. S.; Moerner, W. E. *Phys. Rev. Lett.* **2005**, *94*, 017402.
(12) Crozier, K. B.; Sundaramurthy, A.; Kino, G. S.; Quate, C. F. *J. Appl. Phys.* **2003**, *94*, 4632−4642.
(13) Grigorenko, A. N.; Roberts, N. W.; Dickinson, M. R.; Zhang, Y. *Nat. Photonics* **2008**, *2*, 365−370.
(14) Stewart, M. E.; Mack, N. H.; Malyarchuk, V.; Soares, J.; Lee, T. W.; Gray, S. K.; Nuzzo, R. G.; Rogers, J. A. *Proc. Natl. Acad. Sci. U.S.A.* **2006**, *103*, 17143−17148.
(15) Liu, G. L.; Lee, L. P. *Appl. Phys. Lett.* **2005**, *87*, 074101.
(16) Malyarchuk, V.; Hua, F.; Mack, N. H.; Velasquez, V. T.; White, J. O.; Nuzzo, R. G.; Rogers, J. A. *Opt. Express* **2005**, *13*, 5669−5675.
(17) Haes, A. J.; Zhao, J.; Zou, S. L.; Own, C. S.; Marks, L. D.; Schatz, G. C.; Van Duyne, R. P. *J. Phys. Chem. B* **2005**, *109*, 11158−11162.
(18) McFarland, A. D.; Young, M. A.; Dieringer, J. A.; Van Duyne, R. P. *J. Phys. Chem. B* **2005**, *109*, 11279−11285.
(19) Dieringer, J. A.; McFarland, A. D.; Shah, N. C.; Stuart, D. A.; Whitney, A. V.; Yonzon, C. R.; Young, M. A.; Zhang, X. Y.; Van Duyne, R. P. *Faraday Discuss.* **2006**, *132*, 9−26.
(20) Hong, G. S.; Li, C.; Qi, L. M. *Adv. Funct. Mater.* **2010**, *20*, 3774−3783.
(21) Yokota, Y.; Ueno, K.; Misawa, H. *Chem. Commun.* **2011**, *47*, 3505−3507.
(22) Lee, S. J.; Guan, Z. Q.; Xu, H. X.; Moskovits, M. *J. Phys. Chem. C* **2007**, *111*, 17985−17988.

(23) Lu, Y.; Liu, G. L.; Kim, J.; Mejia, Y. X.; Lee, L. P. *Nano Lett.* **2005**, *5*, 119−124.
(24) Wood, T. H. *Phys. Rev. B* **1981**, *24*, 2289.
(25) Zhang, W. H.; Cui, X. D.; Yeo, B. S.; Schmid, T.; Hafner, C.; Zenobi, R. *Nano Lett.* **2007**, *7*, 1401−1405.
(26) Kao, P.; Malvadkar, N. A.; Cetinkaya, M.; Wang, H.; Allara, D. L.; Demirel, M. C. *Adv. Mater.* **2008**, *20*, 3562−3565.
(27) Wells, S. M.; Polemi, A.; Lavrik, N. V.; Shufordb, K. L.; Sepaniak, M. J. *Chem. Commun.* **2011**, *47*, 3814−3816.
(28) Hirai, Y.; Yabu, H.; Matsuo, Y.; Ijiro, K.; Shimomura, M. *Chem. Commun.* **2010**, *46*, 2298−2300.
(29) Lee, S. Y.; Kim, S. H.; Heo, C. J.; Hwang, H.; Yang, S. M. *Phys. Chem. Chem. Phys.* **2010**, *12*, 11891−11868.
(30) Hartlen, K. D.; Athanasopoulos, A. P. T.; Kitaev, V. *Langmuir* **2008**, *24*, 1714−1720.
(31) Park, S. G.; Lee, S. Y.; Jang, S. G.; Yang, S. M. *Langmuir* **2010**, *26*, 5295−5299.
(32) Heo, C. J.; Jeon, H. C.; Lee, S. Y.; Jang, S. G.; Cho, S.; Choi, Y.; Yang, S. M. *J. Mater. Chem.* **2012**, *22*, 13903−13907.
(33) Lee, S. Y.; Kim, S. H.; Jang, S. G.; Heo, C. J.; Shim, J. W.; Yang, S. M. *Anal. Chem.* **2011**, *83*, 9174−9180.
(34) Choi, D. G.; Yu, H. K.; Jang, S. G.; Yang, S. M. *J. Am. Chem. Soc.* **2004**, *126*, 7019−7025.
(35) Heo, C. J.; Kim, S. H.; Jang, S. G.; Lee, S. Y.; Yang, S. M. *Adv. Mater.* **2009**, *21*, 1726−1731.
(36) Wan, L. J.; Terashima, M.; Noda, H.; Osawa, M. *J. Phys. Chem. B* **2000**, *104*, 3563.
(37) Yu, Q. M.; Guan, P.; Qin, D.; Golden, G.; Wallace, P. M. *Nano Lett.* **2008**, *8*, 1923.
(38) Kneipp, K.; Wang, Y.; Kneipp, H.; Perelman, L. T.; Itzkan, I.; Dasari, R.; Feld, M. S. *Phys. Rev. Lett.* **1997**, *78*, 1667−1670.
(39) Gersten, J.; Nitzan, A. *J. Chem. Phys.* **1980**, *73*, 3023−3037.
(40) Fromm, D. P.; Sundaramurthy, A.; Schuck, P. J.; Kino, G.; Moerner, W. E. *Nano Lett.* **2004**, *4*, 957−961.
(41) Park, S. G.; Lee, S. K.; Moon, J. H.; Yang, S. M. *Lab Chip* **2009**, *9*, 3144−3150.
(42) Lee, S. K.; Park, S. G.; Moon, J. H.; Yang, S. M. *Lab Chip* **2008**, *8*, 388−391.
(43) Lim, C.; Hong, J.; Chung, B. G.; DeMello, A. J.; Choo, J. *Analyst* **2010**, *135*, 837−844.
(44) Quang, L. X.; Lim, C.; Seong, G. H.; Choo, J.; Do, K. J.; Yoo, S. K. *Lab Chip* **2008**, *8*, 2214−2219.

■ NOTE ADDED AFTER ASAP PUBLICATION

This paper was published on the Web on January 8, 2013, with minor errors to the first author's name. The corrected version was reposted on January 10, 2013.